ENG. Struct. Civ. Eng. 2026, 20(10): 1890–1903
https://doi.org/10.1007/s11709-026-1345-1

RESEARCH ARTICLE

Multifunctional sodium-based solid-state structural battery for strengthening and energy storage in near-surface mounted reinforced concrete structures

M. AGHABAGLOO[a], A. J. THATTIL[a], M. CABARROCAS[b], M. BAENA[a], A. EL-FAKDI[b], M. H. BRAGA[c], L. CARRERAS[a*]

[a] *AMADE Research Group, University of Girona, Girona 17003, Spain*
[b] *eXiT Institute, University of Girona, Girona 17003, Spain*
[c] *MatER Research Group, University of Porto, Porto 4200-465, Portugal*
[*] *Corresponding author. E-mail: laura.carreras@udg.edu*

© The Author(s) 2026. This article is published with open access at link.springer.com and journal.hep.com.cn

ABSTRACT The retrofitting of ageing reinforced concrete (RC) structures typically relies on Near-Surface Mounted (NSM) strengthening with carbon fiber reinforced polymers (CFRPs), which provide mechanical enhancement but no additional functionality. To address the growing demand for sustainable, multifunctional solutions, this work introduces a sodium ion based solid-state structural battery that simultaneously serves as a strengthening and energy storage element in NSM applications. The system combines a CFRP shell, providing strength and stiffness, with an embedded sodium-based glass electrolyte exhibiting piezoelectric, pyroelectric and ferroelectric properties. Comprehensive mechanical and electrical characterisation confirmed the multifunctionality of the electrolyte, while pull-out tests on concrete blocks demonstrated effective load transfer, bond behaviour, and failure modes under service conditions. The results validate the dual role of the proposed device, providing both structural reinforcement and energy storage capability, with added potential for structural health monitoring through piezoelectric response. This approach offers a novel pathway towards multifunctional retrofitting strategies for RC structures, integrating mechanical strengthening with energy harvesting and storage.

KEYWORDS NSM strengthening, RC, sodium-based solid-state battery, structural battery, energy storage

1 Introduction

Achieving sustainability in building and construction requires innovative strategies that ensure safety, serviceability, and extended lifespan of structures without compromising environmental and economic viability. In recent decades, the demand for sustainable solutions has become more urgent due to the accelerated deterioration of ageing civil infrastructures. Reinforced concrete (RC), one of the most widely used construction materials, is particularly susceptible to degradation from aggressive environments, corrosion of embedded reinforcement, increased service load requirements, and design or construction deficiencies [1]. Bridges, parking structures, offshore platforms, and residential and commercial buildings worldwide face challenges associated with reduced performance, raising safety concerns and imposing significant maintenance costs [2]. Consequently, the rehabilitation and strengthening of RC structures has emerged as a critical field of research and practice in civil engineering.

Several conventional methods exist for strengthening RC structures, including steel or concrete jacketing, external post-tensioning, externally bonded (EB) steel plates, and the replacement of degraded members [3]. While effective in improving load-bearing capacity, these techniques present notable disadvantages. Steel and concrete jacketing, for example, increase the dead load of the structure, alter cross-sectional dimensions, and require extensive construction time, which may interfere with the

Article history: Received Oct 17, 2025; Accepted Apr 7, 2026

usability of the structure [4]. Similarly, EB steel plates, although relatively simple to apply, are prone to corrosion and debonding, reducing their long-term effectiveness [5]. Such limitations underscore the need for alternative strengthening technologies that are efficient, durable, lightweight, and compatible with the principles of sustainable development.

Fiber reinforced polymers (FRPs) have emerged as one of the most promising alternatives for the rehabilitation of RC structures due to their high strength-to-weight ratio, excellent corrosion resistance, and ease of application [6]. Two major methodologies dominate FRP- strengthening: the EB technique and the near-surface mounted (NSM) technique. The EB method, which involves bonding FRP laminates to the surface of the concrete, has been widely implemented in practice due to its simplicity. However, EB systems suffer from issues such as premature debonding, poor long-term durability when exposed to environmental agents, and possible aesthetic concerns in architectural applications [7]. The NSM technique, by contrast, involves cutting grooves into the concrete cover and inserting FRP strips or rods, which are subsequently bonded with adhesive materials [8]. This approach has gained popularity in recent years because it offers improved bond performance, enhanced protection against environmental degradation, and minimal interference with the appearance of the structure. Moreover, in NSM strengthening the reinforcement is better anchored within the concrete section, leading to improved structural efficiency [9–11]. The NSM technique has therefore become a focal point in research on advanced RC strengthening strategies.

Parallel to advances in structural engineering, recent years have seen a growing emphasis on multifunctionality in materials science. Multifunctionality refers to the integration of multiple roles within a single material or component, thereby optimizing resource use and contributing to sustainability [12]. One promising area of multifunctionality is the development of structural batteries, which combine load-bearing capacity with electrochemical energy storage [13–15].

Structural batteries can be classified into two principal approaches[16]. The first approach develops materials or components that inherently provide both structural and electrochemical functions, thus reducing weight and volume. The second approach treats the structural battery as a hybrid system, where the outer casing bears the mechanical load while the embedded electrochemical system primarily serves as the energy storage medium [14]. Furthermore, designs can be categorized at the cell level, in which battery cells are sandwiched between reinforcing layers, or at the material level, where truly multifunctional components simultaneously serve as structural elements and active battery components [17–19].

Most research on structural batteries has focused on lithium-ion batteries (LIBs), given their high energy and power density, excellent cycling stability, and well-established technology base. However, LIB-based structural systems face critical challenges when applied in civil engineering contexts. Safety issues arise from the flammable liquid electrolytes, which pose risks under mechanical stress or impact loading. In addition, repeated lithiation and delithiation cycles degrade carbon fiber or graphite electrodes, potentially compromising structural integrity [20]. The limited operational temperature range of LIBs further restricts their application in infrastructure, which is often subjected to harsh environmental conditions. High material costs and the need for sophisticated battery management systems also hinder widespread adoption of LIB-based multifunctional systems in large-scale structural applications. Furthermore, civil structures must last decades, while LIBs degrade after10–15 years or even faster under extreme conditions: humidity, temperature cycles, and vibrations drastically reduce LIB lifespan.

To overcome the limitations of LIBs, research has increasingly turned to all-solid-state electrolytes (ASSBs), particularly lithium- and sodium-rich anti-perovskite systems. ASSBs are generally non-flammable and more stable under mechanical stress, making them inherently safer in long-term structural applications. ASSBs are more resistant to mechanical abuse, with ASSBs potentially offering structural reinforcement rather than weakening under stress. Also, ASSBs promise longer lifespans and better tolerance to temperature variations, though real-world data is still emerging, which makes them more compatible with the multi-decade requirements of civil infrastructure.

Among SSBs technologies, sodium-based glass electrolytes (Na^+-glass batteries) are especially promising for structural battery applications. Such electrolytes exhibit ferroelectric behaviour, and, therefore, piezoelectric and pyroelectric properties, enabling multifunctional roles beyond simple energy storage [21]. Recent studies have reported their potential use as strain sensors and dynamic vibration sensors, where the generated electrical signal under mechanical excitation could provide information for structural health monitoring [22]. Moreover, sodium is not only far more abundant and cost-effective than lithium, but also significantly more environmentally benign.

Despite these advantages, several hurdles remain for the widespread use of ASSBs in multifunctional applications. These include challenges associated with electrochemical stability, interfacial resistance, physical contact between solid particles, and large-scale manufacturing [23]. Nonetheless, sodium-based glass electrolytes offer a pathway towards safer and more versatile structural batteries with integrated sensing and energy harvesting functionalities.

While significant research has been conducted on structural batteries in aerospace and automotive applications [19,24], their potential for civil infrastructure remains largely unexplored. At the same time, the rehabilitation of RC structures demands innovative solutions that are not only structurally effective but also contribute to broader sustainability goals. The integration of multifunctional structural batteries into RC strengthening systems provides a unique opportunity to address both challenges simultaneously. Combining a carbon fiber reinforced polymer (CFRP) shell with a sodium-based solid-state electrolyte offers a dual-function system: the CFRP provides the necessary stiffness and strength for NSM reinforcement, while the embedded electrolyte enables energy storage, harvesting, and sensing functionalities. Preliminary studies have demonstrated the electrochemical performance and multifunctional behaviour of sodium ion based glass electrolytes [25], but their application within RC strengthening systems has not yet been investigated.

In this context, the present work introduces a novel structural battery concept for the NSM strengthening of RC elements. The system integrates a CFRP shell, which provides stiffness and mechanical reinforcement, with a sodium ion solid-state glass electrolyte, which enables energy storage and electromechanical sensing. The objective is to develop and characterize this multifunctional reinforcement, assessing its structural, electrochemical, and sensing performance when applied to RC elements.

The paper is organised as follows. Section 2 presents the functional requirements, design rationale, material selection, and manufacturing process of the structural battery. Section 3 describes the experimental programme, including electrical monitoring, mechanical testing of standalone batteries, pull-out testing of batteries embedded in concrete blocks, and *X*-ray computed tomography (CT) inspection. Section 4 reports and discusses the results of these investigations, while Section 5 summarises the main conclusions and outlines directions for future research.

2 Design and development of the structural battery

2.1 Functional requirements

The structural battery developed in this work derives from the coaxial cell architecture proposed by Danzi et al. [25]. In that design, an aluminium rod serves as the cathode current collector, a sodium-based solid electrolyte ($Na_{2.99}Ba_{0.005}OCl$) provides ionic conduction [26], and a copper foil functions as the anode current collector, all encapsulated within a CFRP shell that supplies the mechanical load-bearing capacity. Building upon this concept, the present study adapts the coaxial battery configuration for application in RC strengthening through the NSM technique. To this end, a set of functional and geometrical requirements was established to ensure that the proposed design satisfies both structural and electrochemical performance criteria.

1) The reinforcement geometry must provide a cavity or inner volume suitable for the integration of the all-solid-state electrolyte, ensuring both containment and mechanical stability.

2) The system should enable potential flexural strengthening, contingent on adequate bond, as inferred from pull-out tests comparable to conventional NSM systems [8], while limiting the added cross-sectional area (direct flexural performance was not assessed in this study).

3) The reinforcement dimensions must conform to groove size limitations and construction tolerances. Following detailing guidance in fib Bulletin 90 [27,28], the minimum groove width and depth should be at least 1.5 times the bar diameter, ensuring adequate adhesive cover for effective bond transfer and to mitigate splitting failures.

4) The external geometry of the reinforcement must promote effective adhesion to the concrete substrate, allowing reliable load transfer along the bonded length.

5) The geometry and composite shell must shield the embedded electrolyte from environmental exposure (e.g., moisture, temperature variation, carbonation, chloride ingress), preserving long-term multifunctionality.

6) The reinforcement should employ simple and repeatable geometries that can be fabricated at scale without specialised tooling.

Within this framework, two reinforcement strategies were considered: 1) unidirectional (UD) and 2) angle-ply (AP) fiber arrangements. In the UD strategy, the majority of fibers are aligned with the tensile stresses in flexural members, thereby maximising stiffness and strength in the principal loading direction. To ensure stability of the shell, a limited number of transverse plies are incorporated to resist hoop stresses and maintain dimensional integrity. This strategy reflects conventional strengthening design in RC. In AP strategy, fibers are oriented at ± 45° enabling the scissoring effect, whereby fibers rotate under axial strain, generating in-plane shear deformation. This mechanism introduces pseudo-ductility, producing a nonlinear stress–strain response with enhanced energy absorption and delayed catastrophic failure. Such behavior is advantageous for civil infrastructure applications, as it reduces the risk of sudden brittle fracture and promotes more damage-tolerant failure modes. However, because the fibers are not aligned with the principal flexural stresses, their maximum potential in carrying loads along the reinforcement direction is not fully exploited.

2.2 Constituent materials and specimen configuration

The conceptual design strategies described above were translated into test specimens made of commercial carbon fiber prepregs. Two types of CFRP shells were manufactured.

1) UD shells were fabricated from XC130-C12UD-300 prepreg, a 300 g/m^2 unidirectional carbon fiber material impregnated with the XPREG® XC130 epoxy resin system. A stacking sequence of $[0_2,90_2,0_2]$ was adopted, which provided longitudinal stiffness in the principal loading direction while also including transverse plies to resist hoop stresses. The resulting shells exhibited an outer diameter of 15.6 mm and a wall thickness of 1.8 mm.

2) AP shells were manufactured using XC130-1232T2-450 (1250) prepreg, a 450 g/m^2 2 × 2 twill weave carbon fiber system based on high-strength TR50S 12k fibers. The stacking sequence $[\pm45°]_6$ was employed to promote the scissoring mechanism associated with pseudo-ductility. This configuration yielded an outer diameter of 15.6 mm and a wall thickness of 1.8 mm. Table 1 summarises the key material properties and configurations of the two CFRP shell types.

Table 1 CFRP shell materials and configuration

Property	UD Laminate	AP Laminate
Fiber orientation	$[0_2/90_2/0_2]$	$[\pm45°]_6$
Fiber areal weight (g/m^2)	300	450
Fiber type	Carbon	Carbon
Prepreg type	XC130-C12UD-300	XC130-1232T2-450 (1250)
Shell outer diameter (mm)	15.6	15.6
Shell wall thickness (mm)	1.8	1.8

Both CFRP shells were designed with a fixed outer diameter of 15.6 mm and a length of 520 mm. The electrochemical functionality of the structural battery was realised through the integration of 0.025 mm copper foil, an aluminium rod with a diameter of 3.8 mm positioned at the centre of the cavity, and the sodium ion based all-solid-state glass electrolyte [26], which filled the internal cavity between the two current collectors. The active cavity filled with electrolyte was deliberately restricted to 100 mm in length, positioned at the midspan of the CFRP shell, corresponding to the region required for electrical and mechanical measurements.

Finally, three specimen families were produced: 1) CFRP shells (UD and AP) co-cured with copper foil, manufactured as control specimens for purely mechanical tensile testing; 2) CFRP shells (UD) co-cured with copper foil and filled with resin for purely mechanical pull-out testing; 3) full structural batteries (UD and AP), consisting of the CFRP shell, copper foil, aluminium rod, and all-solid-state electrolyte, designed to investigate multifunctional behaviour.

2.3 Manufacturing of the test specimens

The CFRP shells were fabricated by layup of prepregs on a cylindrical steel mould with a diameter of 12 mm, finished to h6 tolerance. Care was taken to avoid prepreg gaps or overlaps, particularly for the $[0_2,90_2,0_2]$ unidirectional configuration. For the $[\pm45°]_6$ laminates, rectangular prepreg sheets were cut from right-angled triangles to achieve the required ±45° fiber orientation.

First, a release film was wrapped around the mould to facilitate demoulding. A 0.025 mm thick copper foil was placed between the CFRP and the release film wrapped on the steel mould, serving as the anode current collector, and was co-cured with the laminate to ensure good bonding and electrical integration. Finally, a peel ply was applied around the prepregs to ensure surface quality and remove excess resin. A strip of tape was added to the peel ply to serve as an initiator for removal after curing. The assembly was sealed with thermo-retractile flex tape, which contracted during heating and provided compaction pressure on the laminate.

The curing cycle consisted of an initial heating ramp at 3 °C/min up to 120 °C, held for 70 min, and then natural cooling in the furnace. After curing, the CFRP tubes were cut to the 520 mm length, and the peel ply was left in place to protect the surface.

The solid-state electrolyte and aluminium rod were introduced in a subsequent stage. The electrolyte was packed into the CFRP cavity using a concentric cylindrical tube to ensure compaction. The aluminium rod was fixed with cylindrical stoppers at both ends, with the upper stopper allowing the rod to protrude. Finally, the assembled batteries were placed in a vacuum oven at 50 °C for 1 h to remove residual humidity and subsequently sealed with epoxy resin to prevent environmental ingress. Since the electrolyte region was positioned at midspan, the remaining hollow sections were filled with SikaBiresin CR75 (resin) and CH75 (hardener) mixed at 100:40, as recommended by the manufacturer [29].

3 Experimental programme

A comprehensive experimental programme was carried out to characterise the multifunctional performance of the developed structural batteries. The campaign comprised three complementary lines of investigation, each described in the following subsections.

Electrical monitoring (Subsection 3.1): A dedicated system was developed to acquire voltage and current during discharge at room and elevated temperatures. These tests provided insight into the electrochemical behaviour of the batteries and enabled evaluation of their pyroelectric response under thermal variation.

Mechanical testing: The structural role of the batteries was assessed through: (i) quasi-static tensile tests (Subsection 3.2) and (ii) constant-load tensile tests on individual batteries (Subsection 3.3), and (iii) quasi-static and (iv) constant-load pull-out tests on batteries embedded in concrete blocks (Subsections 3.4 and 3.5, respectively). Tensile testing characterised the stiffness and strength of the battery alone, while constant-load tests were combined with electrical monitoring to evaluate piezoelectric effects under sustained loading. Pull-out testing enabled assessment of bond behaviour, failure modes, and load–slip response, with constant-load pull-out tests performed at service-level conditions (30% of the mean ultimate load) to examine the coupled electrical response during realistic structural operation. In the following, the tested specimens are identified using the format *X*–*Y*–*Z*, where *X* refers to the specimen type (SHR for CFRP shell filled with resin and SHB for structural battery), *Y* denotes the fiber orientation (UD for unidirectional laminates and AP for angle-ply laminates), and *Z* represents the order of repetitive similar tests (1, 2, 3, 4).

Internal inspection (Subsection 3.6): Given the handmade nature of the specimens, *X*-ray CT was used to visually inspect the compactness and distribution of the electrolyte within the CFRP cavity, providing valuable information on manufacturing quality.

3.1 Electrical monitoring

Electrical testing commenced with cyclic charge–discharge operations to polarize the structural battery. Each cycle consisted of charging at a constant voltage of 1.5 V for one minute, followed by a one-minute discharge through an external 10 kΩ resistor. After four such cycles, the battery was charged for 30 min at 1.5 V to establish a stable discharge voltage plateau. Once this plateau was achieved, mechanical loading was applied. The transitions between charging and discharging phases were controlled automatically using a digital relay module.

During each charge–discharge cycle, the battery's electrical characteristics (voltage and current) were monitored alongside ambient temperature, given its significant impact on electrochemical performance. The complete experimental setup, illustrated in Fig. 1, comprised an Arduino Uno R3 microcontroller, sensors for electrical and thermal measurements, a dedicated temperature sensor, an external resistor, charging and discharging components, and a software framework for data acquisition and analysis.

High-precision sensors were used to monitor both electrical and thermal parameters. An INA219 current/voltage sensor provided voltage measurements with a resolution of 6.1 mV and current measurements with a resolution of 0.1 mA, transmitting data to the Arduino via I^2C communication. To enhance accuracy during low-current discharge, an N-Fuse tiny Current sensor was incorporated, converting current into an analog voltage signal with a precision of 4.88 μA. Ambient temperature was recorded using an LM35DT sensor, which outputs a voltage proportional to temperature with an accuracy of ±0.5 °C.

A commercial DC power supply was used to provide constant voltage charging at 1.5 V, while discharging was performed through a 10 kΩ external resistor. The transition between charging and discharging phases was managed by a digital relay module, triggered by the microcontroller based on predefined time intervals or voltage thresholds.

Data acquisition and analysis followed a three-tier workflow. First, the Arduino board was programmed to execute cycles every two seconds, acquiring sensor data and transmitting it via the serial port. The program also

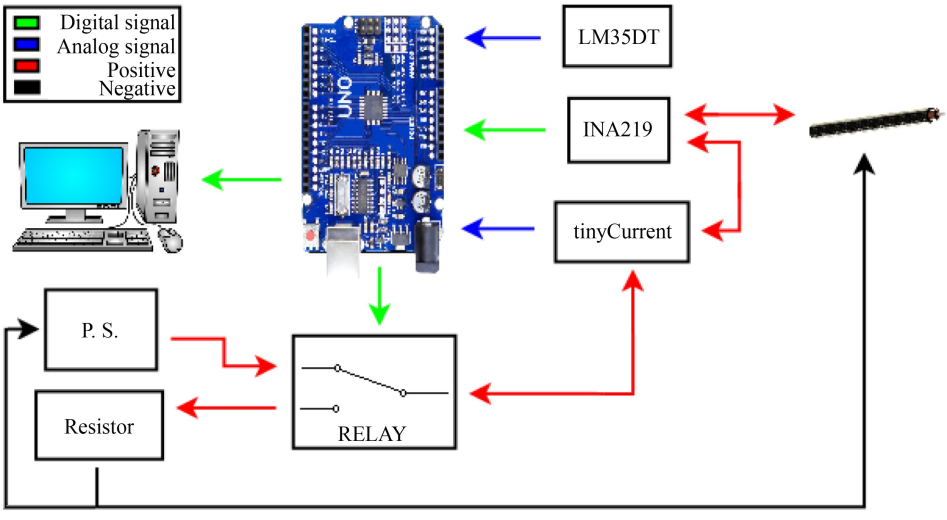


Fig. 1 Electrical test setup.

controlled the relay module, initiating discharge once the specified charging condition was satisfied. Second, Simulink was employed for real-time data reception, conversion, and visualization. Finally, all data were transferred to MATLAB for post-processing, where scripts compiled the results, generated plots, and exported the processed datasets.

3.2 Quasi-static tensile tests on individual batteries

Quasi-static tensile testing was performed to determine the mechanical properties of the structural batteries. Tests followed ISO 10406-1 [30] with a displacement rate of 0.016 mm/s and data acquisition interval of 1 Hz. Specimens SHB-UD and SHB-AP were tested using a 600 kN Universal Hydraulic Testing Machine.

To grip the specimen and prevent local crushing of the CFRP tubes, steel caps of length 150 mm were bonded to both ends, resulting in a gauge length of 220 mm. The caps had an outer diameter of 30 mm and an inner diameter of 20 mm. Four strain gauges were mounted in both hoop and axial directions along the gauge length to monitor deformation. The test specimen and experimental setup are shown in Fig. 2.

3.3 Constant load tests on individual batteries

Constant-load tensile tests were conducted on SHB-UD and SHB-AP specimens to evaluate the coupling between mechanical loading and electrical response, validating the piezoelectric behaviour of the structural battery.

Electrical connections were established by soldering wires to the copper and aluminium electrodes. Steel caps were bonded at both ends and threaded externally for mounting in the constant-load frame. Both electrical (voltage, current, temperature) and mechanical (strain) data were recorded. Three axial strain gauges were installed at the top, center, and bottom of the gauge length, with the outer gauges 50 mm from each end. Cork foil was wrapped around the specimens to isolate the electrolyte from environmental moisture and to suppress pyroelectric interference.

The testing procedure was divided into three stages.

1) Cyclic charging/discharging. Four cycles of 1 min charging at 1.5 V followed by 1 min discharging through a 10 kΩ resistor, with 2 s acquisition interval; no mechanical load applied.

2) Constant-voltage charging. A 30 min charging at 1.5 V to stabilize the voltage plateau; no mechanical load applied.

3) Mechanical loading. An instantaneous stepwise application of constant tensile load; the resulting electrical response was monitored.

The constant-load test specimen and experimental setup are presented in Fig. 3.

3.4 Quasi-static pull-out tests on batteries embedded in concrete blocks

Pull-out tests were conducted to evaluate the bond

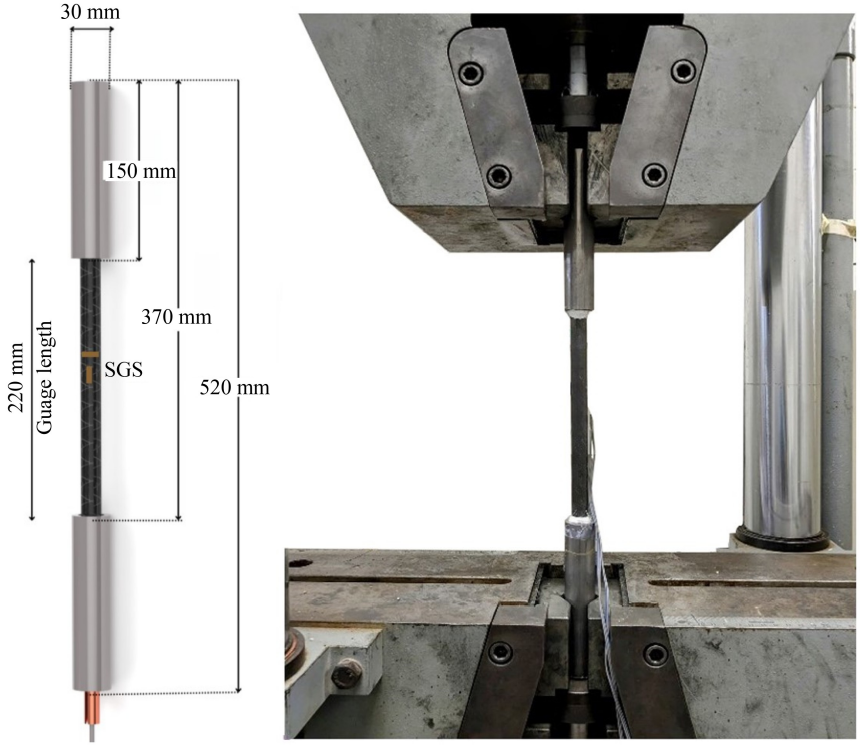


Fig. 2 Experimental configuration for the tensile tests: (a) specimen geometry and instrumentation; (b) tensile test setup.

behaviour of the structural batteries when applied to concrete using the NSM technique. Ready-mix concrete with a compressive strength of 37.9 MPa and an elastic modulus of 27.3 GPa (characterised from 150 mm × 300 mm cylindrical specimens according to UNE 12390-3 [31] and ASTM C469/C469M-10 [32]) was used.

For the pull-out tests, 200 mm × 200 mm × 400 mm concrete blocks were prepared. Grooves measuring 21 mm × 21 mm × 400 mm were machined into the blocks, and structural batteries (SHB-UD & SHR-UD) were bonded using S&P Resin 220 HP epoxy adhesive, mixed at a 2:1 resin-to-hardener ratio and cured for seven days [29]. The bonded length was set to 220 mm, while the free end of the CFRP was kept with a constant unbonded length of 50 mm across all specimens (Fig. 4(a)). The specimens were tested under displacement-controlled conditions using an electromechanical testing machine, at a loading rate of 0.2 mm/min. The corresponding load–slip responses were recorded for each test. A linear variable differential transformer (LVDT) was employed to measure the relative displacement (slip) between the CFRP shell and the concrete substrate, with data sampled at a frequency of 1 Hz. The quasi-static pull-out test specimen and experimental setup are shown in Fig. 4.

3.5 Constant load pull-out tests on batteries embedded in concrete blocks

Constant-load pull-out tests (SHB-UD) were performed to assess the coupled electro-mechanical response of the structural batteries under service-level conditions. The same 200 mm × 200 mm × 400 mm concrete blocks with 21 mm × 21 mm × 400 mm grooves and bonding

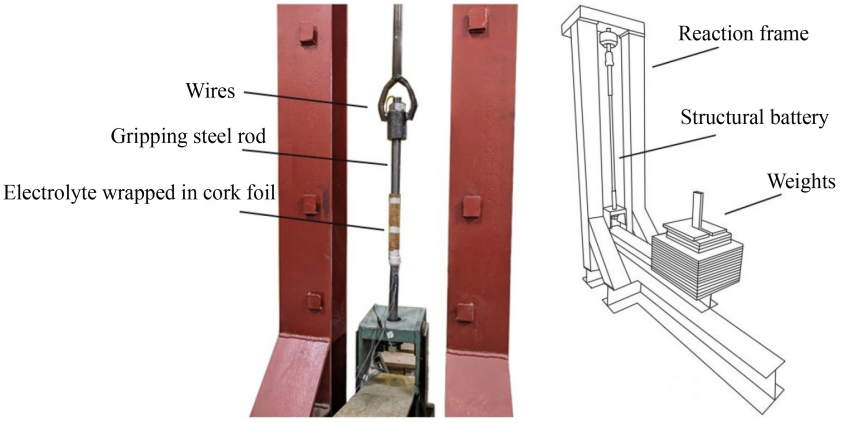


Fig. 3 Constant-load testing configuration of the structural battery: (a) test specimen and loading arrangement; (b) schematic of the experimental setup.

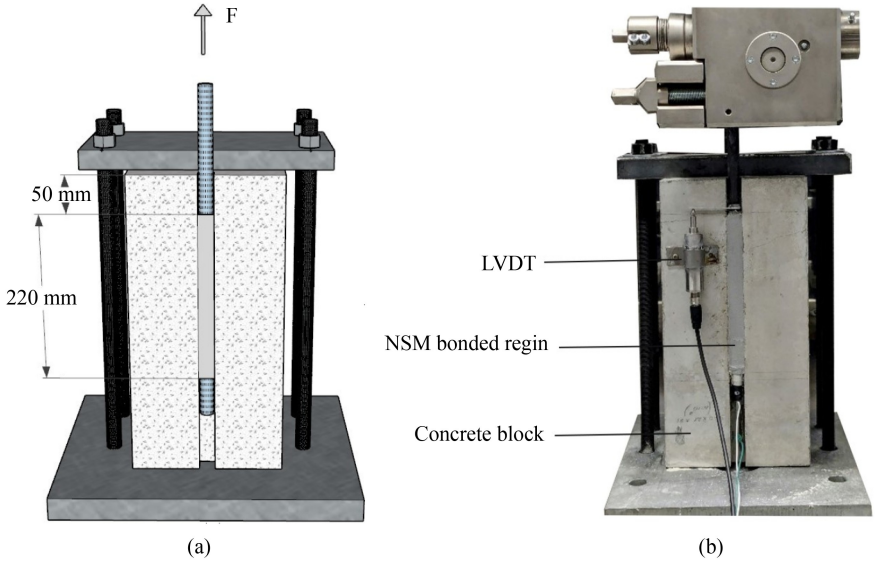


Fig. 4 Pull-out testing configuration of the structural battery embedded in concrete: (a) specimen geometry and bonded region; (b) experimental test setup.

procedure described for the quasi-static tests (Section 3.4) were used.

The tests were conducted at 30% of the mean ultimate load obtained from the quasi-static pull-out tests. Seven strain gauges were installed along the bonded length prior to batteries embedding, enabling detailed monitoring of the strain distribution along the battery length during the test. Testing was carried out in a single-shear configuration with upper confinement by a steel plate (Fig. 4). Slip at the loaded end was measured using a 5 mm gauge-length LVDT, sampled at 1 Hz.

Specimens were loaded under displacement control (0.2 mm/min) until reaching the plateau load, held for 10 minutes, and then unloaded at the same rate. Electrical characteristics were recorded continuously during loading, holding, and unloading.

3.6 X-ray computed tomography inspection

Due to the physical constraints of the tomography setup, the hollow CFRP shells were sectioned to allow inspection of the electrolyte-filled region. The scans were performed using a micro-computed tomography (μ-CT) system equipped with a Hamamatsu L10101 *X*-ray source (maximum power 20 W, 5 µm focal spot) and a Hamamatsu C7942CA-22 high-resolution flat-panel detector (2400 × 2400 pixel CMOS sensor, 50 µm pixel size, 120 mm × 120 mm active area). Scanning was conducted at 55 kV and 110 µA with an exposure time of 1.5 s per projection. A total of 1500 projections were acquired, each with three integrations, yielding a voxel size of 25.059 µm and a field of view of 56.132 mm. The source-to-detector distance (SDD) was 225.470 mm, while the source-to-object distance (SOD) was 113 mm. The acquired data were reconstructed using *X*-AID software and subsequently post-processed with ImageJ for image enhancement and analysis.

4 Results

This section presents the results of the experimental campaign, structured into four main parts: electrical behaviour of the structural battery (Subsection 4.1), mechanical characterisation of the CFRP shells and multifunctional response under constant load (Subsection

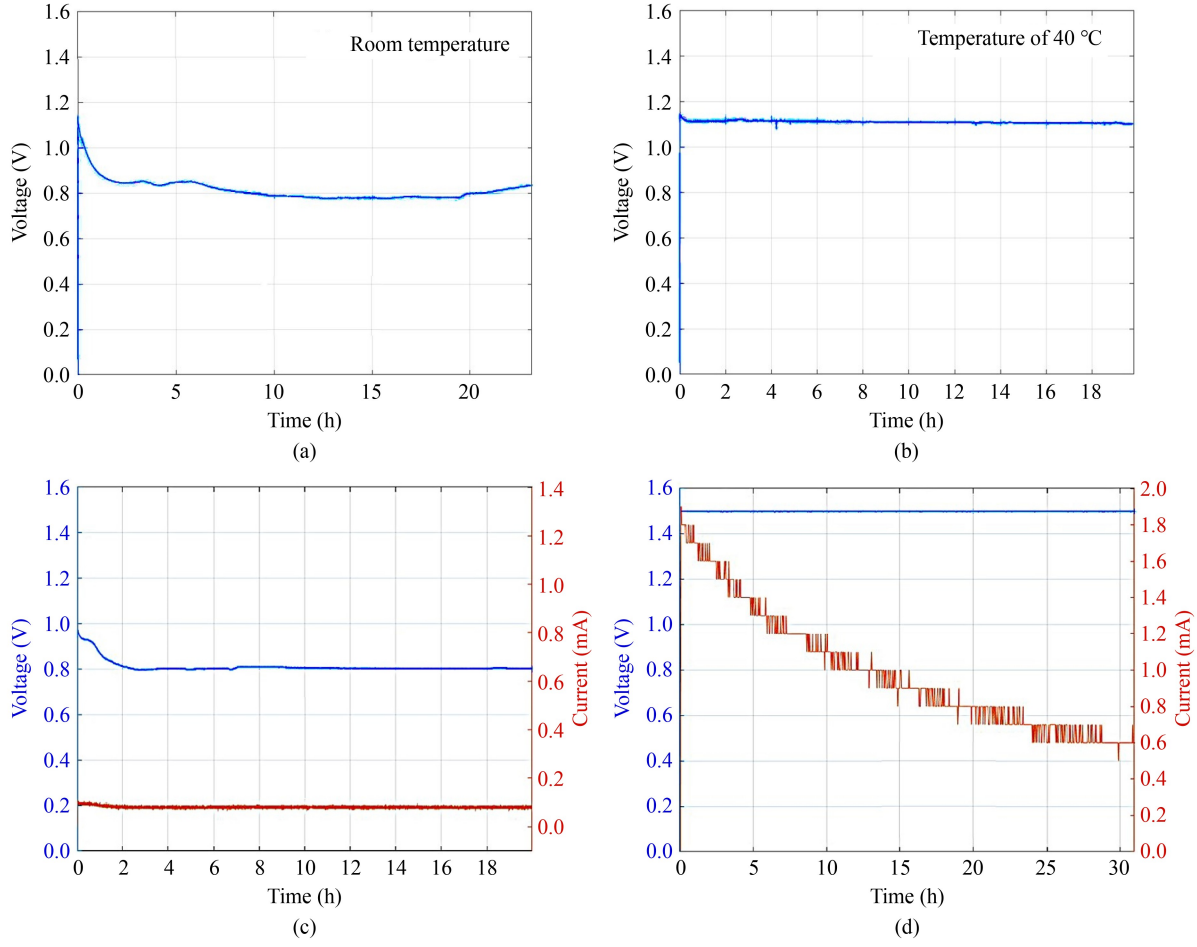


Fig. 5 Test specimen SHB-UD-1: (a) voltage discharge at room temperature; (b) voltage discharge at 40 °C; (c) voltage discharge with current; (d) current curve as temperature gradually falls from 40 to 26.6 °C.

4.2), and bond behaviour in RC elements assessed through pull-out tests (Subsection 4.3), internal inspection of manufactured specimens (Subsection 4.4).

4.1 Electrical characteristics

The electrical monitoring system was employed to record voltage–time discharge curves for the SHB-UD-1 specimen at both room temperature and an elevated temperature of 40 °C. At room temperature, the discharge curves exhibited a pronounced initial voltage drop, attributed to the cell's internal resistance (Fig. 5(a)). At 40 °C, this drop was less pronounced (Fig. 5(b)), confirming the reduction of internal resistance with increasing temperature.

The combined voltage–current response during discharge is presented in Fig. 5(c), where the stepwise variations in current correspond to charge–discharge cycles and reflect the system's electrochemical dynamics. Extended discharge tests further revealed voltage fluctuations associated with day–night ambient temperature variations, reinforcing the temperature dependence of internal resistance.

Finally, when the battery was charged at 1.5 V and maintained at 40 °C using heating tape, subsequent cooling from 40 to 26.6 °C produced a progressive current decrease under constant voltage (Fig. 5(d)), consistent with the increase in resistance at lower temperatures. These results highlight the pyroelectric effect of the sodium-based electrolyte and underscore the pronounced thermal sensitivity of structural battery performance.

4.2 Mechanical characteristics

4.2.1 Tensile properties of CFRP shells

Quasi-static tensile tests were performed on structural batteries with unidirectional (UD) and angle-ply (AP, $[\pm 45]_6$) laminates. The stress–strain curves and failure modes are shown in Fig. 6.

UD laminates. A maximum load of 149.03 kN was recorded for the SHB-UD-02 specimen prior to rupture, corresponding to an ultimate tensile strength of 1989.7 MPa. The measured modulus of elasticity was 115.8 GPa with a low Poisson's ratio of 0.07, validated analytically

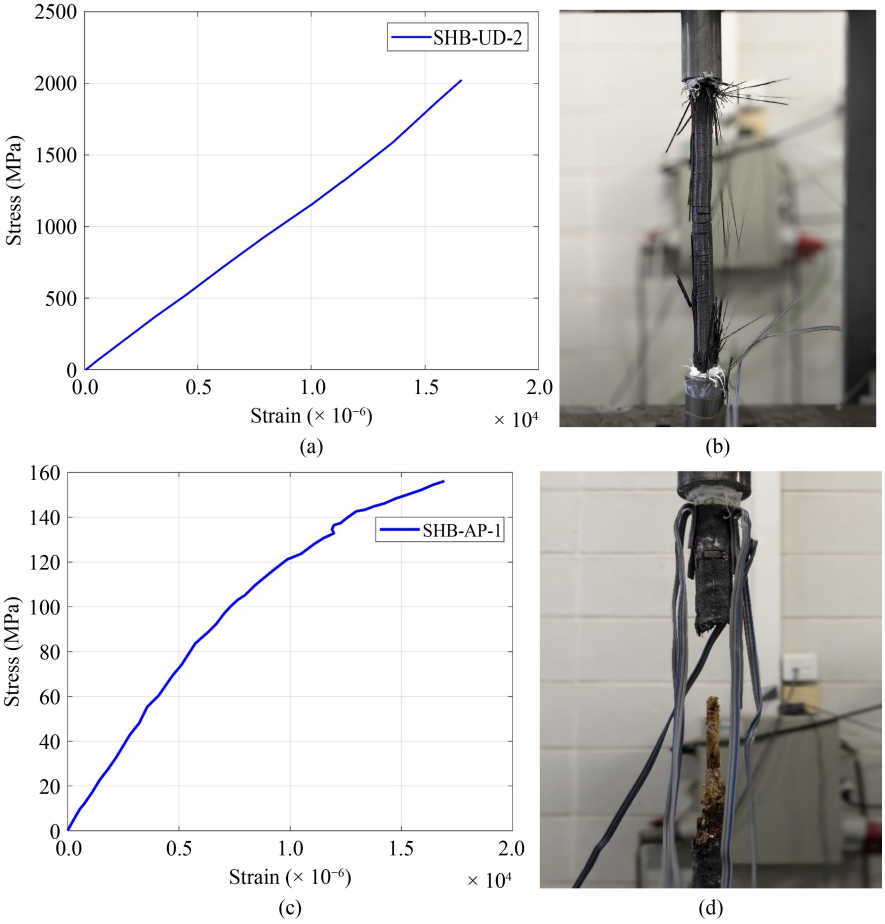


Fig. 6 Stress-strain curves and failure modes: (a) stress vs axial strain for SHB-UD-2 test specimen; (b) failure mode for the SHB-UD-02 specimen; (c) stress vs strain for SHB-AP-1 test specimen; (d) failure mode for the same.

and via strain gauge measurements. Failure was characterised by brittle fiber breakage in the 0° plies (Figs. 6(a) and 6(b)).

AP laminates. A maximum load of 17.58 kN was recorded for the SHB-AP-1 specimen, with an ultimate tensile strength of 200 MPa and a modulus of 15 GPa. Failure initiated near the resin–electrolyte interface (Figs. 6(c) and 6(d)).

Compared to UD specimens, AP laminates sustained only 11.8% of the load and were almost eight times less stiff, but their failure was gradual and non-explosive, a desirable feature for structural applications where brittle fracture must be avoided.

4.2.2 Piezoelectric response under constant load

Constant-load tensile tests were conducted to investigate the electromechanical coupling of the structural batteries and to validate the piezoelectric response of the sodium ion based electrolyte. The procedure followed the three stages described in Subsection 3.3.

1) Cyclic charging/discharging. Four cycles of 1 min charging at 1.5 V followed by 1 min discharging through a 10 kΩ resistor were performed. The voltage response showed the expected periodic rise and fall, while current displayed corresponding polarity changes (Fig. 7(a)). Minor fluctuations in current readings were attributed to sensor resolution.

2) Constant charging. A 30-min charging phase at 1.5 V was applied to establish a stable plateau before loading (Fig. 7(b)).

3) Mechanical loading. Stepwise tensile loading was applied, and the corresponding voltage variation was recorded.

For UD specimens (SHB-UD-1), mechanical loading produced a clear drop in potential from 0.704 to 0.685 V (Fig. 8(a)). Unloading resulted in partial recovery, although the initial level was not fully regained, likely due to strain-induced changes in ion diffusion or electrode damage. With applied mechanical strain in the longitudinal direction, the effect was more pronounced, with no plateau reached before loading (Fig. 8(b)). Comparison with strain gauge measurements confirmed the correlation between mechanical strain and voltage variation (Fig. 8(c)).

For AP specimens (SHB-AP-2), the opposite trend was observed: an increase in potential under loading (Fig. 9). This behaviour is attributed to the high apparent Poisson's ratio (≈ 0.7) of the angle-ply configuration, which arises from fiber rotation under axial loading. The associated transverse contraction induces radial compression of the embedded electrolyte, thereby enhancing dipole polarisation and increasing the observed potential. The specimen attained higher plateau voltages until eventual failure. These results confirm that the structural battery can act as a strain-sensitive element, with laminate architecture strongly influencing the sign and magnitude of the piezoelectric response: UD laminates exhibit voltage drops under load, while AP laminates show voltage increases.

4.3 Bond behaviour from pull-out tests

Pull-out tests were conducted to evaluate the performance of structural batteries as NSM reinforcements in concrete blocks. In quasi-static pull-out tests, a CFRP tube filled with resin (used to minimize the Poisson effect associated with its hollow section) reached an ultimate load of 63.0 kN at a slip of 1.134 mm, failing within the concrete, whereas a structural-battery specimen reached 73.3 kN at 0.968 mm slip (Fig. 10). The observed load–slip response and concrete-governed failure mode are consistent with established NSM pull-out behavior reported in the literature for single-shear, and the measured capacities fall within typical ranges documented for NSM CFRP–concrete joints [33,34].

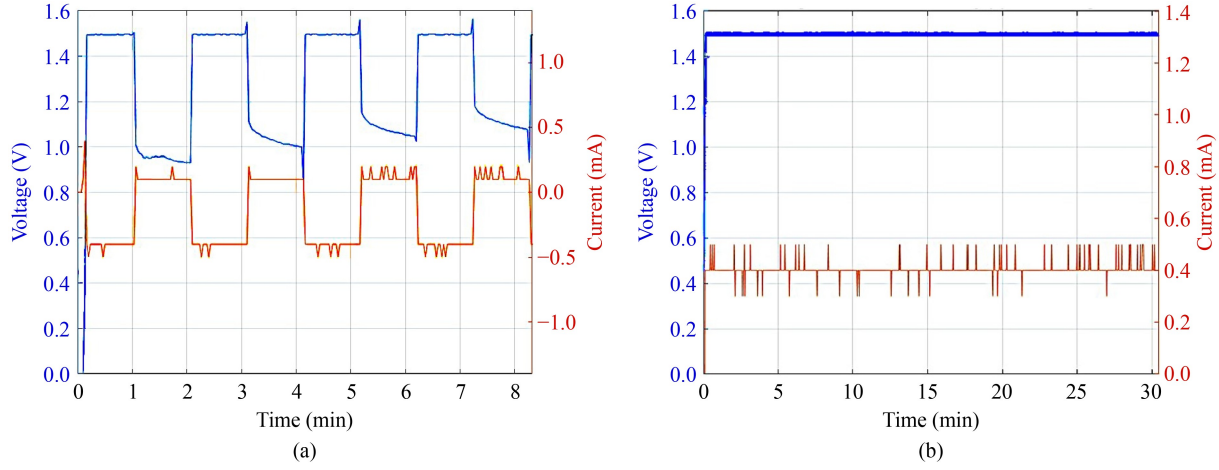


Fig. 7 Electrochemical response of the SHB-UD-1 specimen: (a) charge–discharge cycles; (b) constant-voltage charging at 1.5 V.

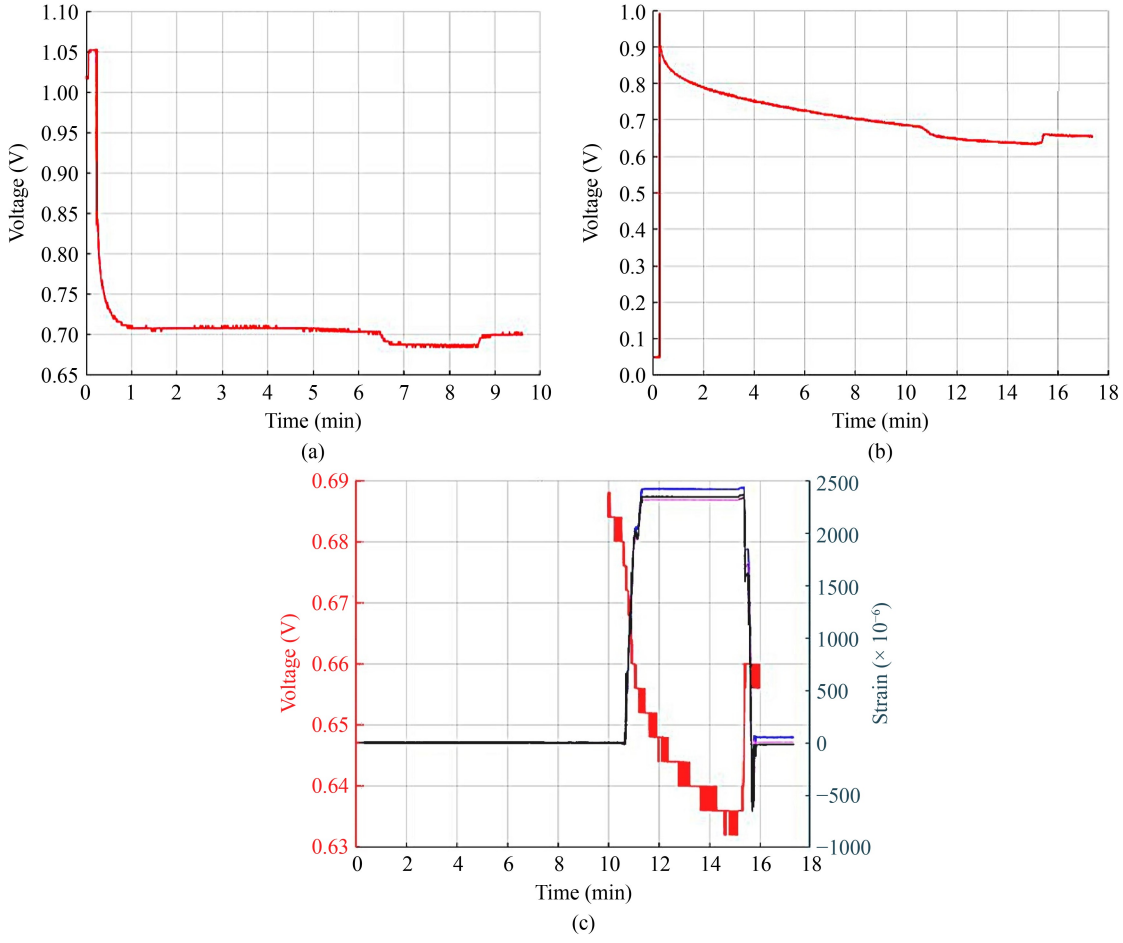


Fig. 8 Constant load curves for SHB-UD-1 test specimen: (a) voltage discharge over time; (b) mechanical loading during voltage discharge; (c) battery response with strain sensor comparison.

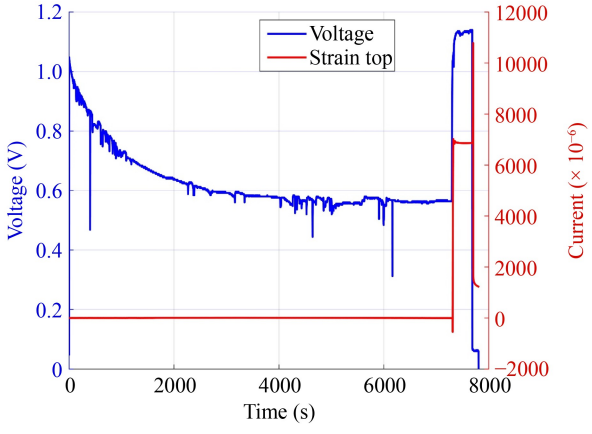


Fig. 9 Constant load test on SHB-AP-2 battery specimen.

Based on the mean maximum load on quasi-static pull-out test, the constant load to be applied to constant-load pull-out tests was determined as 21.5 kN (30% of mean maximum quasi-static load). For specimen SHB-UD-4, the electrical response remained stable under service-level constant loading (Fig. 11(a)), while strain gauge measurements revealed a non-uniform strain distribution along the bonded length, indicating force transfer from the reinforcement to the concrete (Fig. 11(b)). The unaltered voltage can be explained by the localized strain near the loaded end, which did not extend over the full effective bond length and therefore did not affect the entire active region of the structural battery.

4.4 Internal inspection by X-ray computed tomography

X-ray CT was employed to examine the internal quality of the structural batteries (SHB-UD-5), with particular focus on the electrolyte region. The reconstructed images (Fig. 12) show distinct material phases: voids within the electrolyte appear as dark regions, the aluminium rod as light grey, and the electrolyte matrix as darker grey tones.

Several manufacturing-induced defects were identified. Numerous voids were detected in the electrolyte, which could influence internal resistance, while a thin layer was observed around the aluminium rod, possibly associated with sodium metal plating while charging. Despite these imperfections, the specimen maintained an open-circuit voltage (OCV) of 1.1 V, demonstrating functional integrity. The influence of these defects on electrochemical performance was not explored in this study but

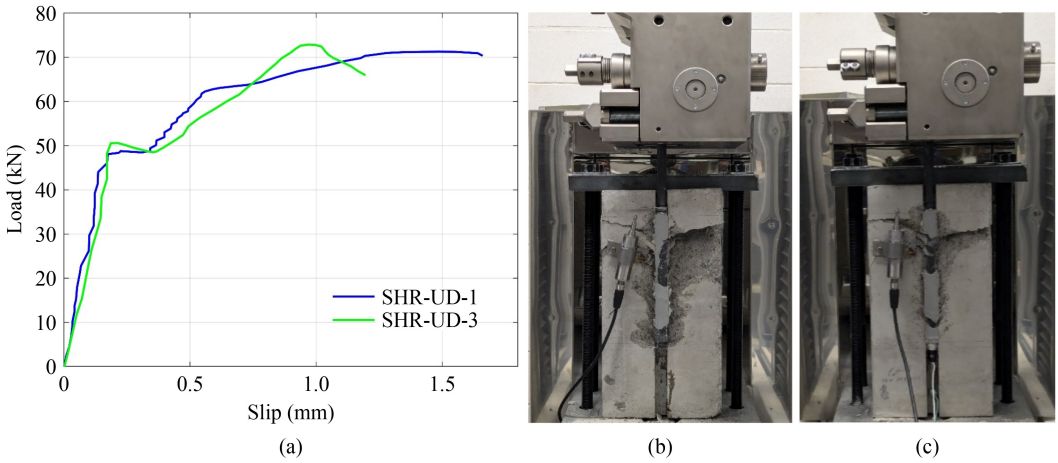


Fig. 10 Pull-out response and failure modes: (a) load–slip curves for CFRP tube SHR-UD-1 and SHB-UD-3 structural battery; (b) CFRP tube failure; (c) structural battery failure.

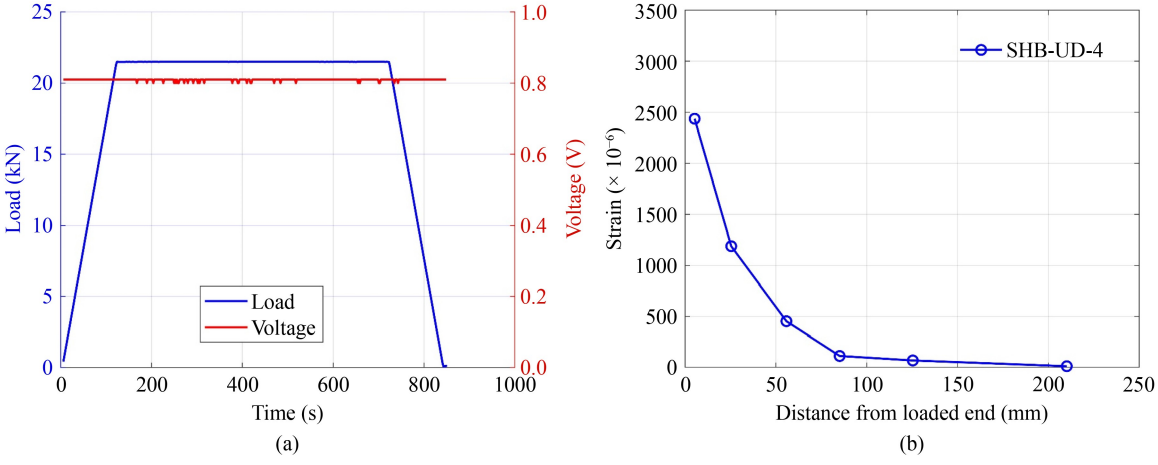


Fig. 11 Electromechanical response under constant load for SHB-UD-4 specimen: (a) load and voltage response; (b) strain profile along the specimen.

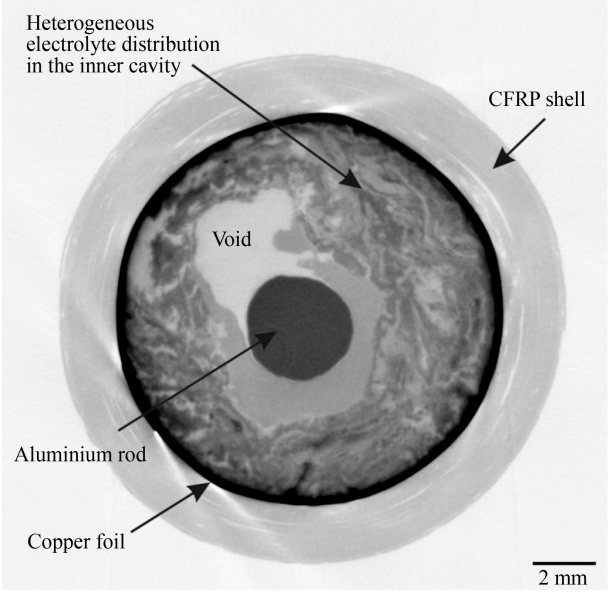


Fig. 12 Tomography scans of specimen SHB-UD-5.

highlights the importance of quality control in future work.

5 Conclusions

This work presented a novel application of sodium ion based all-solid-state structural batteries as multifunctional reinforcement elements for concrete structures. The study covered battery development, electrical monitoring, mechanical and electrochemical characterization, and integration into RC through NSM strengthening. The main conclusions are as follows.

1) The structural batteries demonstrated both pyroelectric and piezoelectric behaviour. Temperature variations modified internal resistance and current flow, while mechanical loading induced measurable voltage changes. The response was highly dependent on laminate architecture: unidirectional laminates exhibited voltage drops under load, whereas angle-ply laminates showed voltage increases.

2) Mechanical testing confirmed the trade-off between stiffness and ductility. Unidirectional laminates provided high strength and stiffness but brittle failure, whereas $[\pm 45]_6$ laminates showed pseudo-ductility at lower strength levels, a behaviour more compatible with RC applications where brittle failure is undesirable.

3) Bond behaviour in concrete confirmed that structural batteries can be effectively applied using the NSM technique. Failure loads were comparable to or higher than conventional CFRP reinforcements, and failure was governed by the concrete rather than the composite, indicating that the electrolyte does not compromise anchorage.

4) Under service-level loading, the batteries maintained a stable electrical potential, demonstrating that structural and electrochemical performance can coexist without conflict.

Overall, the results provide proof of concept for the multifunctional use of sodium-based structural batteries in civil infrastructure. They highlight the potential of this technology to simultaneously provide strengthening, energy storage, and sensing, paving the way for future research on hybrid laminate designs, manufacturing optimization, and long-term durability under realistic service conditions.

Acknowledgements This work was supported by the Spanish Ministry of Science, Innovation and Universities (MICIU/AEI/10.13039/501100011033) through project TED2021-132198B-I00, and by the European Union 'NextGenerationEU'/PRTR; L.C. acknowledges the grant RYC2021-032171-I funded by MICIU/AEI/ 10.13039/501100011033 and by the European Union 'NextGenerationEU'/PRTR.

Funding note Open Access funding provided thanks to the CRUE-CSIC agreement with Springer Nature.

Open Access This article is licensed under a Creative Commons Attribution 4.0 International License (https://creativecommons.org/licenses/by/4.0/), which permits use, sharing, adaptation, distribution and reproduction in any medium or format, as long as you give appropriate credit to the original author(s) and the source, provide a link to the Creative Commons licence, and indicate if changes were made. The images or other third party material in this article are included in the article's Creative Commons licence, unless indicated otherwise in a credit line to the material. If material is not included in the article's Creative Commons licence and your intended use is not permitted by statutory regulation or exceeds the permitted use, you will need to obtain permission directly from the copyright holder. To view a copy of this licence, visit http://creativecommons.org/licenses/by/4.0/.

Competing interests The authors declare that they have no competing interests.

References

1. Broomfield J P. Corrosion of Steel in Concrete: Understanding, Investigation and Repair. 3rd ed. London: CRC Press, 2023
2. Neville A M. Properties of Concrete. 4th ed. Hoboken: Wiley, 1996
3. International Federation for Structural Concrete (fib). Externally Bonded FRP Reinforcement for RC Structures. fib Bulletin 14. 2001
4. Seible F, Priestley M J N, Hegemier G A, Innamorato D. Seismic retrofit of RC columns with continuous carbon fiber jackets. Journal of Composites for Construction, 1997, 1(2): 52–62
5. Garden H N, Hollaway L C. An experimental study of the failure modes of reinforced concrete beams strengthened with prestressed carbon composite plates. Composites Part B: Engineering, 1998, 29(4): 411–424
6. Teng J G, Chen J F, Smith S T, Lam L. FRP: Strengthened RC Structures. Chichester: John Wiley & Sons, 2002
7. Smith S T, Teng J G. FRP-strengthened RC beams. I: Review of debonding strength models. Engineering Structures, 2002, 24(4): 385–395
8. de Lorenzis L, Teng J G. Near-surface mounted FRP reinforcement: An emerging technique for strengthening structures. Composites Part B: Engineering, 2007, 38(2): 119–143
9. Ceroni F, Pecce M, Bilotta A, Nigro E. Bond behavior of FRP NSM systems in concrete elements. Composites Part B: Engineering, 2012, 43(2): 99–109
10. de Sena Cruz J M, de Barros J A O. Bond between near-surface mounted carbon-fiber-reinforced polymer laminate strips and concrete. Journal of Composites for Construction, 2004, 8(6): 519–527
11. Barros J A O, Fortes A S. Flexural strengthening of concrete beams with CFRP laminates bonded into slits. Cement and Concrete Composites, 2005, 27(4): 471–480
12. Gibson R F. A review of recent research on mechanics of multifunctional composite materials and structures. Composite Structures, 2010, 92(12): 2793–2810
13. Thomas J P, Qidwai M A. The design and application of multifunctional structure-battery materials systems. JOM, 2005, 57(3): 18–24
14. Asp L E, Johansson M, Lindbergh G, Xu J, Zenkert D. Structural battery composites: A review. Functional Composites and Structures, 2019, 1(4): 042001
15. Ladpli P, Nardari R, Kopsaftopoulos F, Chang F K. Multifunctional energy storage composite structures with embedded lithium-ion batteries. Journal of Power Sources, 2019, 414: 517–529
16. Danzi F, Salgado R M, Oliveira J E, Arteiro A, Camanho P P, Braga M H. Structural batteries: A review. Molecules, 2021, 26(8): 2203
17. Leijonmarck S, Carlson T, Lindbergh G, Asp L E, Maples H, Bismarck A. Solid polymer electrolyte-coated carbon fibres for structural and novel micro batteries. Composites Science and Technology, 2013, 89: 149–157
18. Asp L E, Greenhalgh E S. Structural power composites. Composites Science and Technology, 2014, 101: 41–61
19. Asp L E, Bouton K, Carlstedt D, Duan S H, Harnden R, Johannisson W, Johansen M, Johansson M K G, Lindbergh G, Liu F, et al. A structural battery and its multifunctional performance.

Advanced Energy and Sustainability Research, 2021, 2(3): 2000093
20. Liu P, Sherman E, Jacobsen A. Design and fabrication of multifunctional structural batteries. Journal of Power Sources, 2009, 189(1): 646–650
21. Braga M H, Grundish N S, Murchison A J, Goodenough J B. Alternative strategy for a safe rechargeable battery. Energy & Environmental Science, 2017, 10(1): 331–336
22. Christoff B G, Marques D, Carmo J P, Braga M H, Tita V. On the strain-sensing capabilities of a novel all-solid-state sodium-based-electrolyte battery under vibration loads. Mechanical Systems and Signal Processing, 2024, 215: 111390
23. Radjendirane A C, Maurya D K, Ren J N, Hou H, Algadi H, Xu B B, Guo Z H, Angaiah S. Overview of inorganic electrolytes for all-solid-state sodium batteries. Langmuir, 2024, 40(32): 16690–16712
24. Kühnelt H, Beutl A, Mastropierro F, Laurin F, Willrodt S, Bismarck A, Guida M, Romano F. Structural batteries for aeronautic applications—State of the art, research gaps and technology development needs. Aerospace, 2021, 9(1): 7
25. Danzi F, Camanho P P, Braga M H. An all-solid-state coaxial structural battery using sodium-based electrolyte. Molecules, 2021, 26(17): 5226
26. Braga M H, Murchison A J, Ferreira J A, Singh P, Goodenough J B. Glass-amorphous alkali-ion solid electrolytes and their performance in symmetrical cells. Energy & Environmental Science, 2016, 9(3): 948–954
27. International Federation for Structural Concrete (fib). Externally Applied FRP Reinforcement for Concrete Structures. fib Bulletin 90. 2019
28. Parretti R, Nanni A. Strengthening of RC members using near-surface mounted FRP composites: Design overview. Advances in Structural Engineering, 2004, 7(6): 469–483
29. S&P Clever Reinforcement Company AG. S&P Resin 220 HP High Performance Epoxy Adhesive. Available online (accessed on 2020)
30. ISO 10406-1:2008. Fiber-Reinforced Polymer (FRP) Reinforcement of Concrete-Test Methods, Part 1: FRP Bars and Grids. Geneva: International Organization for Standardization, 2008
31. EN 12390-3:2009. Testing Hardened Concrete-Part 3: Compressive Strength of Test Specimens. Madrid: AENOR, 2011
32. ASTM C469/C469M-10. Standard Test Method for Static Modulus of Elasticity and Poisson's Ratio of Concrete in Compression. West Conshohocken, PA: ASTM, 2010
33. Aghabagloo M, Carreras L, Barahona M, Barris C, Baena M. Experimental study and numerical prediction of the bond-slip law for concrete elements strengthened with FRP using metaheuristic algorithm. Construction and Building Materials, 2024, 411: 134712
34. Emara M, Barris C, Baena M, Torres L, Barros J. Bond behavior of NSM CFRP laminates in concrete under sustained loading. Construction and Building Materials, 2018, 177: 237–246